A Physical Model to Estimate Snowfall over Land using AMSU-B Observations

[1,2] Min-Jeong Kim, [3]J. A. Weinman, [4,5]W. S. Olson, [6]D.-E. Chang,[1]G. Skofronick-Jackson, and [1]J. R. Wang

[1]NASA Goddard Space Flight Center, Code 614.6, Greenbelt, MD 20771
[2]Cooperative Institute of Research in Atmospheric Sciences, Colorado State University, Fort Collins, CO
[3]Department of Atmospheric Sciences, University of Washington, Seattle, WA 98195
[4]Joint Center for Earth Systems Technology, University of Maryland Baltimore County
[5]NASA/Goddard Space Flight Center, Code 613.1, Greenbelt, MD 20771
[6]Forecast Research Laboratory, Meteorological Research Institute, Korea

Journal of Geophysical Research

To be submitted to

Journal of Geophysical Research

Corresponding author address:

Min-Jeong Kim

NOAA/NESDIS/STAR

Room #712

5200 Auth Road
Camp Springs, MD 20746

Abstract

In this study, we present an improved physical model to retrieve snowfall rate over land using brightness temperature observations from the National Oceanic and Atmospheric Administration's (NOAA) Advanced Microwave Sounder Unit-B (AMSU-B) at 89 GHz, 150 GHz, 183.3±1 GHz, 183.3±3 GHz, and 183.3±7 GHz. The retrieval model is applied to the New England blizzard of March 5, 2001 which deposited about 75 cm of snow over much of Vermont, New Hampshire, and northern New York.

In this improved physical model, prior retrieval assumptions about snowflake shape, particle size distributions, environmental conditions, and optimization methodology have been updated. Here, single scattering parameters for snow particles are calculated with the Discrete-Dipole Approximation (DDA) method instead of assuming spherical shapes. Five different snow particle models (hexagonal columns, hexagonal plates, and three different kinds of aggregates) are considered. Snow particle size distributions are assumed to vary with air temperature and to follow aircraft measurements described by previous studies.

Brightness temperatures at AMSU-B frequencies for the New England blizzard are calculated using these DDA calculated single scattering parameters and particle size distributions. The vertical profiles of pressure, temperature, relative humidity and hydrometeors are provided by MM5 model simulations. These profiles are treated as the a priori data base in the Bayesian retrieval algorithm. In algorithm applications to the blizzard data, calculated brightness temperatures associated with selected database profiles agree with AMSU-B observations to within about ±5 K at all five frequencies. Retrieved snowfall rates compare favorably with the near-concurrent National Weather Service (NWS) radar reflectivity measurements. The relationships between the NWS radar measured reflectivities Z_e and retrieved snowfall rate R for a given snow particle model are derived by a histogram matching technique. All of these Z_e-R relationships fall in the range of previously established Z_e-R relationships for snowfall. This suggests that the current physical model developed in this study can reliably estimate the snowfall rate over land using the AMSU-B measured brightness temperatures.

1. INTRODUCTION

Falling snow is an important component of the global water cycle. Heavy snowfall can disrupt transportation flow and cause subsequent severe flooding. Snow packs accumulated on the ground serve as a reservoir of water for agriculture and hydroelectric power generation. Moreover, falling snow that persists as snow cover over land can affect earth energy balance through a change in the surface albedo. Understanding extratropical precipitation is critical for improving the prediction capability of regional and large-scale climate models for the water cycle. For the last several decades, ground-based radars and snow gauges have been used to monitor snowfall rate. However, spatial coverage of radar and snow gauge networks outside of the USA, Europe, and Japan is sparse. Snowfall rate measurements from space can overcome this spatial sampling limit and provide data sets necessary for the improvement of weather forecasting, hydrological and climate research.

While satellite-based rain rate estimates are reliable and operational (Olson et al. 1996; Ferraro el al. 2005; Olson et al. 2006), the measurement of snowfall rates from space is a relatively new field (Chen and Staelin 2002; Kongoli et al 2003; Skofronick-Jackson et al. 2004; Liu 2004, Noh et al. 2006). There are two major challenges associated with retrieving snowfall rates (a) adequately representing and retrieving the complex macro and microphysical features of snow clouds, and (b) distinguishing surface features from atmospheric signatures. The measurement of snowfall within the atmosphere has been difficult using radiometers that operate at frequencies below 100 GHz where the atmosphere is relatively transparent and the surface emissivity can

produce brightness temperatures (Tb) expected from precipitating clouds. Indeed, retrievals of snow pack rely on the 19 and 37 GHz channels (Foster et al. 2005). Recently, falling snow retrievals have been derived from spaceborne microwave radiometry over oceanic regions where the measurements are not affected by surface snow (Weinman and Hakkarinen 1990; Liu and Curry 1996; Schols et al. 1999; Bennartz and Petty 2001).

Passive microwave radiometers operating at frequencies near 183 GHz, such as NOAA's Advanced Microwave Sounder Unit-B (AMSU-B), and those on proposed satellites like the Global Precipitation Mission (GPM) and the Meteorological Operational Mission (METOP) polar orbiting satellites, can minimize the surface emission problem over land because water vapor absorption effectively masks the surface emission. For example, AMSU-B operating at 89 GHz, 150 GHz, 183.3±7, ±3, and ±1 GHz has been employed to estimate frozen hydrometeors (Chen and Staelin 2002; Kongoli et al 2003; Skofronick-Jackson et al. 2004; Noh et al. 2006). Kongoli et al. (2003) derived snowfall over land from the AMSU-B Tbs using empirical relationships. Chen and Staelin (2003) employed a neural network technique in their snowfall retrievals. Although such empirical relationships or statistical techniques may be operationally useful, physical models are needed to understand how the measured Tbs depend on various surface and atmospheric parameters.

Skofronick-Jackson et al. (2004) developed a physical model at millimeter-wave frequencies from which snowfall rates over land could be inferred. While their snowfall

rate retrievals were qualitatively validated, the retrievals are greatly enhanced by improving the assumptions.

- That study approximated the single scattering properties of snow crystal as equal volume (V) to area (A) ratio spheres (Grenfell and Warren 1999). In the IR/UV frequency regions, the methods using the equal-V/A spheres generally do not provide accurate estimates of the asymmetry factors (Takano and Liou 1988; Grenfell and Warren 1999). Recent analyses by Liu (2004) and Kim (2004) demonstrated the limitation of such an approach at microwave frequencies. A refined technique to calculate the scattering properties of non-spherical snow particles is employed herein.
- In addition, the particle size distribution (PSD) of equal-V/A spheres employed in the early study was simplified over the vertical height of the cloud. In this work, PSDs are taken from in-situ observations of snowflakes over the vertical domain of clouds.
- Another simplifying assumption in the previous study was the number of atmospheric and hydrometeor profiles used in the retrievals. Only 11 and 36 representative profiles of relative humidity and snow water content, respectively, were extracted from mesoscale model simulations. Additionally, the model simulation resolution from the earlier study was 40 km × 40 km, which is much larger than the AMSU-B footprints (~ 16 km × 16 km at nadir). To obtain more realistic retrievals, the number and diversity of atmospheric profiles needed to be expanded and the resolution of the simulated data improved.

- Further, the method of Skofronick-Jackson et al. (2004) was to find a final profile that minimized the differences between the observed Tbs and calculated Tbs without any consideration of the correlation between model variables (e.g. very low relative humidity was retrieved with heavy snowfall). The current study uses a Bayesian method for optimizing the retrievals and correlations between variables are considered in retrievals. Noh et al.(2006) also developed a Bayesian method based algorithm to retrieve the froze precipitation retrievals using high frequency microwave satellite data. However, their study did not consider error correlations between different channels so that only diagonal terms of the error covariance matrix were employed in the Bayesian algorithm. In this study, the correlations between the retrieved variables are considered. Modeling errors are obtained from systematic Tb sensitivity tests, based upon the uncertainties of several parameters, including particle size, water vapor content, ice content, and surface emissivity.

The purpose of this study is to improve the retrieval algorithm for estimating snowfall rate with millimeter-wave channels. The major improvements from this study are given below. First, the Discrete-Dipole Approximation (DDA) method (Purcell and Pennypacker 1973; Draine and Flatau 2003) is employed to calculate more precisely the single scattering parameters of nonspherical snow crystals in radiative transfer calculations. Second, snow particle size distributions are based on in-situ observations by Houze et al (1979), Lo and Passarelli (1982), and these distributions are allowed to vary with height. Third, an a priori data base containing appropriate and realistic simulated

profiles is created for snowfall parameter retrievals within a Bayesian methodology. In addition, an error analysis and sensitivity tests are performed.

The paper is organized as follows: The blizzard snow storm case considered in this study is briefly described in section 2; radar and AMSU-B observations as well as MM5 simulated cloud profiles are also presented. Details of the a priori database are explained in Section 3. The retrieval methodology including the Bayesian method is described in section 4. Retrieval results and uncertainty analysis are presented in Section 5. Finally, summary and conclusions are given in Section 6. In the Appendix, the sensitivity of the AMSU-B radiometer to humidity and precipitation profiles and surface snow coverage are examined by calculating Jacobians (after Bauer and Mugnai 2003).

2. SNOWSTORM CASE: *Northeastern Blizzard on March 5, 2001*

The snowstorm considered in this study is the blizzard of March 5-6, 2001 over the Northeastern United States. This is the same blizzard case reported by Skofronick-Jackson et al. (2004). The blizzard deposited about 75 cm of snow over much of Vermont, New Hampshire, and northern New York during its lifetime. Figure 1(a) shows a composite of the National Weather Service (NWS) operational weather radar reflectivity March 5, 2001 at 2300 UTC. The NWS radar reflectivity data were averaged over 16 km × 16 km grid template to match the finest spatial resolution of the AMSU-B channels. The maximum reflectivity in the smoothed radar reflectivity data over land is ~40 dBZ.

Shown in Figures 1(b)-(f) are the Tbs measured by the AMSU-B on the National Oceanic and Atmospheric Administration (NOAA)-15 satellite at 2302 UTC on March 5, 2001. The AMSU-B is a cross-track scanner with an angular swath of $\pm 50^{o}$. The southeast to northwest intense snow band is at about 35^{o} off nadir. It is noted that the 89 GHz channel shows ambiguity in distinguishing snow in the atmosphere from other surface features on the ground such as lakes, rivers, and snow on the ground. On the other hand, the 183 GHz channels (especially those closest to the water vapor line center) can screen the surface effect except in the driest atmospheric conditions such as those found in the arctic.

3. GENERATION OF A PRORI DATA BASE

3.1 Mesoscale model simulation

In the retrieval algorithm, vertical profiles of pressure, temperature, relative humidity, cloud ice, cloud water, and hydrometeor profiles are derived from the MM5 model (Grell et al. 1994) which was used to the Northeastern Blizzard at 4 km resolution. The MM5 model was initialized at 00 UTC on March 5, 2001 and the model integration was performed for a period of 24 hours. The simulation domain with 36 km resolution was nested to the domain with 12 km resolution and then to the domain with 4 km resolution. The model domain was centered at 35° N and 70° W and consisted of 231 × 231 grid points at 4 km resolution. These profiles were linearly averaged to 16 km × 16 km resolution to match the AMSU-B foot print size at nadir.

The Goddard scheme (Tao and Simpson 1993) was used for ice microphysics parameterizations in the simulations. All the temperatures near the surface over New England were below –2 °C and the observations are at 19:00 local time; therefore, the precipitation was either snow or graupel over land. Graupel generated by the MM5 model over land was converted to snow of equivalent water content in this study because the National Lightning Detection Network (NLDN) observed some lightning off-shore, but not over New England.

In addition to the MM5-generated profiles at 16 km × 16 km resolution, assumed fractional surface snow cover values of 0, 0.1, 0.2, …, 1.0 are used as input to forward radiative transfer calculations to adjust the surface emissivity. Thus, the surface varies from 100 % mixed bare soil/frozen soil/winter forest to 100 % snow cover. Employing these input profiles and calculated Tbs in an *a priori* database, a Bayesian algorithm is used to retrieve atmospheric environment and hydrometeor profiles and surface snow cover fraction using AMSU-B observed Tbs. Details of the scattering parameterizations, particle size distributions, snow particles' orientation, radiative transfer calculations, and the Bayesian retrieval framework are presented in the following sections.

*3.2 Single scattering parameter of snow particle*s

The Discrete Dipole Approximation (DDA) method was used to compute single scattering parameters of various idealized nonspherical snow crystals which were then used in the Tb calculations. The DDA method is a flexible technique for calculating the electromagnetic scattering and absorption by particles with arbitrary shapes and

composition (Draine 1988; Mishchenko et al. 2000). The DDA treats the actual particle as an array of dipoles. Each of the dipoles is subject to an electric field which is the sum of the incident wave and the electric fields due to all of the other dipoles. Through the solution of the electric field at each dipole position, the scattering and absorption properties of the particle are obtained. The DDA replaces a solid particle with an array of point dipoles occupying positions on a cubic lattice, and the lattice spacing must be small compared to the wavelength of the incident radiation. Therefore, the DDA method requires large computer storage and CPU time. The technique is not well suited for particles with very large complex refractive indices because it requires much narrower distance between dipoles, thus requiring much larger memory size. This study employs the DDA codes developed by Draine and Flatau (2003).

The five idealized snow crystal models considered in this study are shown in Figure 2: hexagonal columns (HC), three types of snow aggregates composed of two cylinders (C2), three cylinders (C3) and four cylinders (C4), and hexagonal plates (HP). Singlescattering parameters of HCs, C2s, C3s, C4s, and HPs were previously calculated by Kim (2006) for the aspect ratio (the ratio of small dimension to large dimension of ice crystals) ~ 0.1.

For this work we changed the aspect ratio to one that had a thinner column based on the observations in the previous studies (Auer and Veal 1970; Heymsfield 1972). Following Auer and Veal (1970) and Heymsfield (1972), the relationship between diameter (D) and length (L) for hexagonal columns is given by

$$D = 0.197 \times L^{0.414} \quad [\text{mm}] \quad (1)$$

The aggregates (C2s, C3s, and C4s) are modeled with two, three, and four circular cylinders having the same aspect ratio as a hexagonal column.

The thickness (T) and width (W) relationship for hexagonal plates follows Auer and Veal (1970) and is given by

$$T = 0.048 \times W^{0.474} \quad [\text{mm}] \quad (2)$$

The density of ice for each cylinder and plate is assumed to be the same as pure ice (0.91 g/m^3). Dielectric constants are calculated with formulas given by Mätzler and Wegmüller (1987).

3.3 Orientation of snowflakes

Single scattering parameters of nonspherical particles strongly depend on the orientation of the particles in the snowfall. Vivekanandan et al. (1994, 1999) showed that differential reflectivities of snow particles measured by polarimetric radar observations were close to zero. Differential reflectivity is the ratio of the horizontal copolar return to the vertical copolar return and can be interpreted as the reflectivity weighted mean-axis ratio of the precipitation particle in the radar resolution volume. Thus it is a good indicator of orientation of particles. This implies that snow particles are randomly oriented in dry snow regions of various precipitating systems. For this reason, snow particles are assumed to be randomly oriented in our analysis.

In addition, the atmosphere was known to be strongly turbulent in the snowstorm under study. Shown in Figure 3 are the profiles of wind speed and Richardson number observed by NWS instrumentation in Brookhaven (41° N, 73° W), New York at 00 UTC on 6 March 2001, an hour after the NOAA-15 AMSU-B observations; This figure shows that wind speed was greater than 10 m/sec with strong wind shear at most altitudes.

The Richardson number, *Ri* (Bluestein 1993), which is a measure of the importance of buoyancy forces to inertial accelerations, is defined as follows:

$$\mathrm{Ri} = \frac{\left(g \frac{\mathrm{d} \ln \theta}{\mathrm{dz}} \right)}{\left(\frac{\mathrm{d} |\mathrm{v}|}{\mathrm{dz}} \right)^2} \qquad (3)$$

where θ is the potential temperature and v is the wind speed. When *Ri* is small (≤ 0.25), the flow becomes turbulent (Bluestein (1993)). Small *Ri* numbers were observed during this storm, suggesting that the atmosphere below 10 km height was turbulent and the particles are randomly oriented.

It should be stressed that this case study is very limited and the random orientation of snow particles assumed here may not be generalized to all snowstorms. For example, Hogan et al. (2002) analyzed simultaneous aircraft and polarimetric radar data for a warm-frontal mixed-phased cloud. By analyzing the differential reflectivity given by $\mathrm{Z_{DR}} = 10 \log_{10} \left(\frac{\mathrm{Z_H}}{\mathrm{Z_V}} \right)$ dB, where Z_H and Z_V are reflectivity factors measured at horizontal and vertical polarizations, respectively, they showed the possibility of horizontal

alignment of the ice crystals in the region of embedded convection where high concentrations of small crystals were observed. More comprehensive observations of the orientation of snow particles using radar and passive microwave radiometer measurements, in-situ snow crystal microphysics samples, atmospheric stability observations, and wind profiles from high resolution soundings are necessary to clarify the particle orientation issue, and to gain a more complete understanding of falling snow retrievals.

3.4 Snow particle size distributions

In-situ microphysics data describing snow crystal shapes and size distributions were not available during this snow storm. Therefore, we employ snow particle size distributions (PSDs) measured by Houze et al. (1979) and Lo and Passarelli (1982) for midlatitude winter storms.

According to these studies, the snow PSDs are represented by exponental functions given by

$$N(D) = N_0 \exp(-\lambda D) \qquad [\mathrm{mm^{-1}m^{-3}}] \qquad (4)$$

where D is the large dimension of snow particle.

By fitting a curve to the data shown in Houze et al. (1979), λ is assumed to follow:

$$\lambda = 10^{-\frac{T}{41}} \qquad [\mathrm{mm^{-1}}] \qquad (5)$$

where T(°C) is the air temperature. It is noted that Eqn.(5) can be used to describe the λ versus air temperature relationship shown in Lo and Passarelli (1982).

3.5 Falling velocity of snow particles

To convert snow water contents to snowfall rates, the following equation by Rutledge and Hobbs (1983) for terminal velocity (V_t) of snow particles is employed:

$$V_t(D) = 1.139 \times D^{0.11} \times (\frac{P_0}{P})^{0.4} \qquad \text{[m/sec]} \qquad (6)$$

where P is atmospheric pressure for a given altitude and P_0 is a reference value equal to 1000 mb (Rutledge and Hobbs 1983). The factor $(\frac{P_0}{P})^{0.4}$ allows for the change in fall speed with air pressure (Foote and DuToit, 1969), such that as the pressure decreases with altitude, the particles fall faster.

Then snowfall rates are calculated using

$$RR(mm/hr) = 6\pi \times 0.91 \times 10^{-4} \int D_{eff}^3 V_t(D) N(D) dD \qquad (7)$$

where D_{eff} [mm] is the diameter of an equal-mass ice sphere corresponding to a given snow particle. The factor of 0.91 is multiplied in Eqn.(7) to convert ice snow to an equivalent volume of liquid water.

3.6 Radiative transfer calculations

The radiative transfer model used to compute Tbs from a hydrometeor profile is the delta-Eddington model (Weinman and Davis 1978, Thomas and Stamnes 1999, Kim et al. 2004). Vertical profiles of pressure, temperature, humidity and hydrometeors are provided by the MM5 model simulations described in Section 3.1. Single scattering coefficients, asymmetry factors, and single scattering albedos of snow particles are calculated with scattering models described in Section 3.2, based upon the particle size distributions described in Section 3.4. Gaseous absorption coefficients for oxygen and

water vapor are obtained from the millimeter propagation model (MPM) of Liebe et al. (1992).

The radiative transfer calculations also require a knowledge of the emissivity of the variable surface features, including snow cover. The boundary conditions were determined partially by the accumulated antecedent snow for which the emissivities ε_s for deep dry snow at a 35° viewing angle are 0.64, 0.724, and 0.8 at 89, 150, and 183 GHz, respectively (Hewison and English 1999). The emissivity used in the radiative transfer model is a weighted mean of the emissivity of snow cover ε_s and ε_0, where ε_0 is an average of the emissivities of bare soil, frozen soil, and winter forest/conifer surfaces. The value of ε_0 is 0.98 for all frequencies based on the observations shown in Hewison et al. (2001). The effective emissivity is thus

$$\varepsilon = \mathbf{f}\varepsilon_s + (1-\mathbf{f})\varepsilon_0 \qquad (8)$$

where **f** is the snow cover fraction that is assigned 11 discrete values: 0.0, 0.1, 0.2, 0.3, 0.4, …., 1.0.

4. RETRIEVAL METHODOLOGY

A Bayesian inversion technique is used to retrieve falling snow profiles. An a priori data base was built using the MM5 generated atmospheric and hydrometeor profiles. For a given snowfall profile, different snow particle shapes (5 kinds) and various surface emissivity values (11 snow cover fractions) were considered in the radiative transfer calculations. That is, 11 different Tbs were generated at each frequency for a given

snowfall profile and a given snow particle type. In-situ microphysics observations of snow particle habits were not available; therefore, the five snow particle models discussed in Section 3.2 are used in the Tb calculations. However, for a given retrieval application to the AMSU-B data, only one shape was allowed at a time due a lack of information about the number and types of particle shapes for this blizzard case. Retrievals assuming different particle shapes are compared.

Following Olson et al. (1996) and Moreau et al. (2003), if it is assumed that the errors in the observations and the simulated observations are Gaussian and uncorrelated then the "best" estimate of state vector x, given the set of observations $\mathbf{y}_0$, is the expected value

$$\mathbf{x_a} = \int\int\ldots\int \mathbf{x}\,\mathbf{exp\{}-0.5\mathbf{[y}_0 - \mathbf{y}_s\mathbf{(x)]}^{\mathrm{T}}\mathbf{(O+S)}^{-1}\mathbf{[y}_0 - \mathbf{y}_s\mathbf{(x)]\}}\mathrm{P}_a\mathbf{(x = x_{true})} / \mathrm{A}\ \mathbf{dx} \qquad (9)$$

where A is a normalization factor,

$$\mathrm{A} = \int\int\ldots\int \mathbf{exp\{}-0.5\mathbf{[y}_0 - \mathbf{y}_s\mathbf{]}^{\mathrm{T}}\mathbf{(O+S)}^{-1}\mathbf{[y}_0 - \mathbf{y}_s\mathbf{(x)]\}}\mathrm{P}_a\mathbf{(x = x_{true})dx}\,. \qquad (10)$$

Here, $y_s(x)$ are simulated Tbs and P_a is the a priori probability that x is the true state profile of the atmosphere. The O and S are the observed and simulated Tb error covariance matrices, respectively.

The inherent uncertainty is given by the integration of departures of the best estimate state vector $\mathbf{x_a}$ from those contained in the database:

$$\mathbf{E(x)} = \int\int\ldots\int \mathbf{(x - x_a)}^2\,\mathbf{exp\{}-0.5\mathbf{[y}_0 - \mathbf{y}_s\mathbf{(x)]}^{\mathrm{T}}\mathbf{(O+S)}^{-1}\mathbf{[y}_0 - \mathbf{y}_s\mathbf{(x)]\}}\mathrm{P}_a\mathbf{(x = x_{true})} / \mathrm{A}\ \mathbf{dx} \qquad (11)$$

When generating the a priori database, the evaluation of the associated modeling uncertainties is difficult but important for both retrievals and error estimation. Tb uncertainties were included in the error covariance matrix representing the intrinsic variability of the generated a priori database. Tassa et al. (2006) proposed a methodology for taking into account cloud-radiation database related modeling uncertainties for precipitation retrieval from the TRMM Microwave Imager (TMI). In their study, the modeling errors were obtained from systematic Tb sensitivity tests, based upon the assumed uncertainties in PSD, atmospheric temperature, ice content, sea surface wind speed, viewing angle, melting phase, and particle shape.

Following Tassa et al. (2006), modeling uncertainties associated with the generation of a priori database were calculated in this study for snowfall retrievals using AMSU-B measurements. The uncertainties were computed through sensitivity analyses aimed at evaluating the impact of various bulk cloud/radiative parameters on the resulting simulated radiance distributions. We assume there are four fundamental sources of error: errors in calculating surface emissivity, errors in calculating scattering parameters, errors in water vapor profiles, and errors in radiative transfer. We address these sources of error as follows:

(a) Regarding surface emissivity, we add Gaussian-distributed errors to our computed emissivity for each emissivity calculation we make in generating the database. The standard deviation of emissivity errors assumed in this study is 0.05.

(b) Even though we consider the Bayesian estimates for each particle habit separately, there still could be errors in each calculation of the single scattering parameters and the size spectra of the hydrometeors that can have a very large impact on snow radiative properties (Panegrossi et al. 1998, Viltard et al. 2000). In this study, we added Gaussian-distributed errors to the mass median diameter of the PSDs described by Eqn.(4). The standard deviation for the percentage error was assumed to be 50 %.

(c) Since AMSU-B brightness temperatures are sensitive to water vapor profiles, we added Gaussian-distributed errors to the MM5 generated water vapor content profiles. The standard deviation of the percentage error was assumed to be 10 % and the error was assumed to be same for all levels.

(d) Because we did not use rigorous a Monte Carlo radiative transfer model because of increased computation time required for these calculations, there will be some uncertainty in radiance calculations that increases in proportion to the effective scattering in the vertical column. Therefore, we calculate a "cloud –free" background Tb and then calculated the difference between the background and cloudy atmosphere Tb. This Tb difference represents the effective scattering by snow in the vertical column. We added a Gaussian-distributed percentage error to the cloudy atmosphere Tb in proportion to a Tb difference. The standard deviation of the percentage error was assumed as 8 %. For example, if the original Tb was 100 K below the background value, then typically we would add or subtract 8 K to the Tb. Since the Tb depressions at 89 GHz and 150 GHz relative to the background can be affected by the low surface emissivity of snow on the ground, errors from source (d) were calculated by assuming surface snow fraction was zero and isolating the Tb depression due to scattering in the atmospheric column.

Errors only from (a) first, and then (b) only, and then (c) only, and then (d) only, and then all four error sources together were calculated. The error covariances due to errors from (a), (b), (c), and (d) are shown in Tables 1-4, respectively. The error covariances calculated with (a), (b), and (c) error sources considered together are shown in Table 5. Finally, each component of Table 4 and Table 5 are summed for the total error covariance (Table 6) which was applied in Eqn. (9) for snow retrievals.

Noh et al. (2006) neglected the error correlations between different channels by assuming the off-diagonal terms of error covariance matrix to be zero. However, this study demonstrates that the modeling error correlations are significantly large between different channels of AMSU-B and emphasizes that they should not be neglected in precipitation retrievals.

Table 1. Computed error covariances (K^2) due to error source (a) surface emissivity

	89 GHz	150 GHz	183.3±7 GHz	183.3±3 GHz	183.3±1 GHz
89 GHz	39.32	16.82	0.33	0.00	0.00
150 GHz	16.82	7.78	0.17	0.00	0.00
183.3±7GHz	0.33	0.17	0.005	0.00	0.00
183.3±3GHz	0.00	0.00	0.00	0.00	0.00
183.3±1GHz	0.00	0.00	0.00	0.00	0.00

Table 2. Computed error covariances (K^2) due to error source (b) snow particle size

	89 GHz	150 GHz	183.3±7 GHz	183.3±3 GHz	183.3±1 GHz
89 GHz	19.45	38.43	6.74	-2.37	-1.15
150 GHz	38.43	89.71	23.57	-0.28	-1.09
183.3±7GHz	6.74	23.57	15.58	6.59	1.67
183.3±3GHz	-2.37	-0.29	1.77	5.57	6.59
183.3±1GHz	-1.15	-1.09	1.67	1.77	0.61

Table 3. Computed error covariances (K^2) due to error source (c) water vapor amount

	89 GHz	150 GHz	183.3±7 GHz	183.3±3 GHz	183.3±1 GHz
89 GHz	8.82	11.72	0.92	-3.16	-4.71
150 GHz	11.72	16.42	1.82	-4.31	-6.60
183.3±7GHz	-0.92	1.82	1.29	0.09	-0.41
183.3±3GHz	-3.16	-4.31	0.09	1.58	2.07
183.3±1GHz	-4.71	-6.60	-0.41	2.07	3.00

Table 4. Computed error covariances (K^2) due to error source (d) radiance computation

	89 GHz	150 GHz	183.3±7 GHz	183.3±3 GHz	183.3±1 GHz
89 GHz	0.86	1.62	0.84	0.57	0.89
150 GHz	1.62	3.15	1.61	1.04	1.56
183.3±7GHz	0.84	1.61	0.88	0.59	0.89
183.3±3GHz	0.57	1.04	0.59	0.47	0.75
183.3±1GHz	0.89	1.56	0.89	0.75	1.25

Table 5. Computed error covariances (K^2) due to error sources (a), (b), and (c)

	89 GHz	150 GHz	183.3±7 GHz	183.3±3 GHz	183.3±1 GHz
89 GHz	70.87	66.79	2.62	-7.92	-6.29
150 GHz	66.79	98.68	9.99	-10.22	-7.66
183.3±7GHz	2.62	9.99	5.77	3.23	1.78
183.3±3GHz	-7.92	-10.22	3.23	5.98	3.88
183.3±1GHz	-6.29	-7.66	1.78	3.88	3.54

Table 6. The error covariances (K^2) employed in the retrievals in this study

	89 GHz	150 GHz	183.3±7 GHz	183.3±3 GHz	183.3±1 GHz
89 GHz	71.73	68.41	3.46	-7.35	-5.4
150 GHz	68.41	101.83	11.60	-9.18	-6.1
183.3±7GHz	3.46	11.60	6.57	3.82	2.67
183.3±3GHz	-7.35	-9.18	3.82	6.45	4.63
183.3±1GHz	-5.4	-6.1	2.67	4.63	4.79

Table 6 shows that modeling errors are strongly correlated between 89 GHz and 150 GHz channels and between 183.3±3 and 183.3±1 GHz channels and correlations coefficients are 0.80 and 0.83, respectively. It is noted that water vapor uncertainties result in Tb errors that are significantly anti-correlated at the lower and higher channel frequencies. That is, more water vapor increases the Tb at 89 GHz but decreases the Tb at 183.3±1 GHz. Table 5 shows that the largest Tb error covariances are associated with the 89 and 150 GHz channels, primarily due to assumed uncertainties in modeled surface emissivities and PSDs.

5. RETRIEVAL RESULTS

5.1 Falling Snow Retrievals

Using the algorithm previously descrbied, retrievals were performed for the March 2001 blizzard case shown in Figure 1. Each retrieved profile contains vertical distributions of temperature, relative humidity, and snow water content. The lowest altitude snow water content (at 20.0 m) is converted to a melted precipitation rate using the procedure described in Section 3.5 (Falling Velocity of Snow Particles), as shown in Figure 4(a). Since the retrieval method was designed for applications over land, the oceanic regions are masked. The snowflake shape employed in the retrievals shown in this figure is HC (Fig. 2). Retrieval results from different snow particle models are compared later in this section. As seen in Figure 4(a), the spatial distribution of retrieved snowfall rates is similar to the radar reflectivity observations displayed in Figure 1(a). Retrieved water equivalent snowfall rates reach a maximum of ~ 4.3 mm/hr, which helps to explain the heavy snowfall accumulations (up to ~75 cm) reported during this storm.

In order to understand the retrievals on a Tb basis, the spatial distributions of differences between the Bayesian retrieved Tbs and the AMSU-B observations at all five frequencies of the storm region are shown in Figure 5. Results show that the computed Tbs agree with the observations within ±5 K over most of the storm region at all of the AMSU-B frequencies.

Using Eqn.(11), the inherent uncertainty of retrievals is calculated by integrating departures of profiles contained in the a priori database from the retrieved profile. The

distribution of error standard deviations related to the retrieved snowfall rates is shown in Figure 4(b). It may be inferred that the uncertainty of the retrieved snowfall rates in this study range between 0.01 and 2 mm/hr at 0.02 km altitude. As shown in Figure 4(c), the error standard deviations increase with the retrieved snowfall rates.

Similar to Figure 4, the retrievals are repeated for each of the five snow particle shapes shown in Figure 2. To compare retrieved snowfall rates using the different snow particle models, a pixel area matching technique similar to that described in Calheiros and Zawadski (1987) is used to relate the radar reflectivity Z_e (mm^6 m^{-3}) observed by NWS radars over land to the retrieved snowfall rate, R at 0.02 km altitude above the surface. The procedure selects a number of pixels that exceed a given snowfall rate and the same number of pixels that exceeded a particular radar reflectivity. Threshold values of each of these quantities are tabulated and plotted in Figure 6 with colors. The black lines in Figure 6 show the Z_e-R relationships for falling snow presented in previous studies such as Sekhon and Srivastava (1970), Fujiyoshi et al. (1990), Vasiloff et al. (2000), Boucher and Weiler (1985), and Skofronick-Jackson et al. (2004).

Comparisons in Figure 6 show that NWS radar observed Z_e versus retrieved R curves of all snow crystal models considered in this study agree well with previously published Z_e-R relationships. Retrieved snowfall rates assuming the C4 snow particle model, yield the smallest values, while retrieval results based upon HCs yield the largest snowfall rate for a given radar reflectivity. Variations of retrieved snowfall rates can differ by a factor of 2. Further, the ranges of uncertainties associated with different

particle shapes enclose all previously published Z_e-R relationships and all snow particle shapes evaluated in this study.

5.2 Consistency Checks

The distribution of fractions of snow cover on the ground selected by the Bayesian retrieval method are shown in Figure 7(a). Within the AMSU-B field of view the snow cover fraction ranges between 0.2 and 0.6 over the snow storm core region. Figure 7(b) shows that the uncertainties (standard deviations) of the snow cover fraction are about 0.15 to 0.2 in the storm core. These higher uncertainties are likely caused by the fact that none of the channels probe to the surface in the heavily precipitating storm core, and hence the Bayesian technique can select wide range of surface snow cover fraction values without affecting the resultant Tbs.

It is noted that retrieved fractions of snow cover over the Great Lakes and St. Lawrence River regions (near 73°W and 46°N) are large. This is a direct result of the 89 GHz channel sensitivity to surface features. The 89 GHz AMSU-B image 48 hours earlier than the time analyzed for the snowfall retrievals and prior to the start of our analyzed snow fall event is shown in Figure 8(a). In this image, a cold surface feature is seen in the same region where the retrieved snow cover fraction is high. Indeed, all the AMSU-B 89 GHz images from March 1-10, 2001 exhibit the same cold brightness temperatures. This region is a river valley with elevations near sea level. To validate of retrieved surface snow coverage in this region, snow water equivalent (SWE) values were derived with the algorithm in Foster et al. (2005) using the Special Sensor Microwave Imager (SSM/I) 19 GHz and 37 GHz vertically polarized channels. The SSM/I retrieved SWE for March 4,

2001 are shown in Figure 8(b), prior to the blizzard analyzed in this work. The SWE distribution provides evidence that there was more snow on the ground near the Great Lakes and St. Lawrence River regions than in other areas before the March 5-6, 2001 blizzard, suggesting that the distribution of retrieved surface snow fraction derived in the current study is valid.

The relative humidity (%) and uncertainties at 0.02 km altitude above the surface in the retrieved profiles are shown in Figure 9. In Figure 9(a), retrieved relative humidity values are large (above 90 %) over the snow storm core region where the radar reflectivity is greater than 30 dBZ (Fig. 1(a)). The uncertainties range up to 7 %. The uncertainties are lower over the region where the retrieved relative humidity values are high. It should be emphasized that the uncertainty here is in reference to the MM5 produced relative humidity profiles. Therefore, the accuracy of the retrieved humidities is limited by the range of humidities in the profiles in the MM5 data base.

Compared to the previous retrieval results of Skofronick-Jackson et al. (2004), the new algorithm retrieves snowfall rate distributions that are more consistent with the NWS radar reflectivity distribution (Fig. 6). It should be noted that the distributions of retrieved parameters such as snow water content and relative humidity in Skofronick-Jackson et al. (2004) were noisy, and that the maximum retrieved snow water content was associated with physically inconsistent low relative humidity profiles in that study. In the current study, the improved physical and statistical assumptions in the retrieval algorithm result in relative humidity values that are relatively high over the snowstorm region, which is consistent with moisture convergence and lifting in this intense storm (Fig. 9).

6. SUMMARY AND CONCLUSIONS

In this study, we improved a snowfall retrieval method by addressing our assumptions described in Skofronick-Jackson et al. (2004) and estimate snowfall rate over land using the AMSU-B Tb observations at 89 GHz, 150 GHz, 183.3±1 GHz, 183.3±3 GHz, and 183.3±7 GHz. This improved retrieval model is applied to the blizzard of March 5, 2001 over New England. Major improvements resulting from this study are following:

- The current study employs the Discrete-Dipole Approximation (DDA) method (Purcell and Pennypacker 1973; Draine and Flatau 2003) to calculate single scattering parameters for various nonspherical snow particles in radiative transfer calculations.
- This study incorporates snow particle size distributions based on in-situ observations by Houze et al (1979), Lo and Passarelli (1982), and vary with height.
- Instead of assuming that the fall velocity is fixed at 1 m/sec for all falling snow particles (Skofronick-Jackson et al. 2004) to convert retrieved snow water content to snowfall rate, this study employs the relationships between fall velocity and snow particle sizes described in Rutledge and Hobbs (1983).
- The current study uses a Bayesian method for optimizing the retrievals and correlations between variables are considered in retrievals. Unlike previous Bayesian retrievals of Noh et al. (2006), the present study accounts for the error covariance of Tbs in retrievals. This reduces the noise that was present

- This study demonstrates that modeling errors are strongly correlated especially between 89 GHz and 150 GHz channels and between 183.3±3 and 183.3±1 GHz channels. Water vapor uncertainties result in Tb errors that are significantly anti-correlated at the lower and higher channel frequencies. The largest Tb error covariances are associated with the 89 and 150 GHz channels, primarily due to assumed uncertainties in modeled surface emissivities and PSDs.

Comparisons of the current retrieved snowfall rates with NWS radar reflectivity measurements indicate better consistency in relation to those of Skofronick-Jackson et al. (2004). This consistency is evaluated in terms of reduced noise in the retrieved distributions, the use of non-spherical snowflake shapes, correlations between variables, a Bayesian inversion method with Tb error covariances between different channels, and the use of realistic surface emissivity variables. Results suggest that the physical model developed in this study uses more appropriate and realistic assumptions and further improves estimates of snowfall rate over land based upon high frequency microwave brightness temperatures.

The results of error analysis show that the uncertainty inherent in the retrievals of snowfall ranges between 0.01 mm/hr and 2 mm/hr at 0.02 km altitude above the surface, increasing with snowfall rate. For retrieved relative humidity, the uncertainty is less than

7 % over the whole retrieval domain, although this uncertainty is more of a measure of the error in the variability of the MM5 relative humidity profiles. Standard deviations of retrieved surface snow coverage over most of the storm area range between 0 and 0.2.

APPENDIX: Sensitivity

The sensitivities of Tbs to variations of humidity, hydrometeor profiles, and surface emissivity, represented by Jacobians, helps to explain the model error covariance derived in section 4: Greater sensitivity of Tbs to a given geophysical parameter means that there is greater model error associated with uncertainties in that parameter. In addition, the analysis of model Jacobians is standard procedure in data assimilation schemes because Jacobians provide crucial information on model sensitivity to input perturbations as a function of model state. Its application to cloud and precipitation parameters via radiative transfer analysis is relatively new (Moreau et al. 2003). It has also influenced radiometer optimization studies outside the NWP community (Bauer and Mugnai 2003). Here, Jacobians associated with relative humidity and hydrometeor profiles, which are extracted out of the MM5 simulations (Section 3.1) over land, are calculated.

Figure A1 and Figure A2 show Jacobians, *J*, for AMSU-B channels with respect to humidity and snow water content profiles, respectively. The *J* units for humidity and snow water content profiles are $\Delta K/\Delta(g/kg)$ and $\Delta K/\Delta(g/m^3)$, respectively. In these figures, solid and dashed lines indicate mean values and standard deviation values,

respectively. The sensitivity of the calculated Tbs to the fraction of snow coverage and snow particle size distributions is presented in Figure A3. The snow particle model used to calculate Tbs shown in these figures is HC (Fig.2).

From Figure A1, it may be noted that the 89 GHz channel is nearly insensitive to water vapor variations, and that the 150 GHz Tbs slightly increase with water vapor increment (< 0.5 K/(g/km)). As we may expect, the water vapor channels (183.3 ± 1, 183.3 ± 3, and 183.3 ± 7 GHz) are sensitive to variation in humidity. In particular, the calculated Tbs are most sensitive to variations of water vapor amount at altitudes around 7 km – 8 km. Considering the water vapor channels, on average, the most opaque channel (e.g., 183.3±1 GHz) is more sensitive to water vapor variations than the least opaque channel (e.g., 183.3±7 GHz).

In Figure A2, the calculated Jacobians show that both the 183.3 ±7 GHz and 150 GHz channels are most sensitive to snow water content. It is also noted that the water vapor channels are not sensitive to the snow water content near the surface, where the calculated Jacobians at 89 GHz and 150 GHz show sensitivities of 1 K/(0.1 g/m^3) and 2.5 K/(0.1 g/m^3), respectively. The 89 GHz, 150 GHz, 183.3 ± 1 GHz, and 183.3 ± 3 GHz, and 183.3 ± 7 GHz channels are most sensitive to the snow water content at 3 km, 4 km, 5 km, 6 km, and 7 km altitudes, respectively. This result suggests a limited snow profiling capability if these channels are combined in a retrieval algorithm and the water vapor connection can be determined or specified independently.

Figure A3 presents histograms of Tb differences (ΔTb) when the fraction of surface snow coverage increases from **f** = 0.5 to **f** = 0.6. From the figure it is seen that the 89 GHz channel is three times more sensitive to the surface snow coverage than the 150 GHz channel, while the water vapor channels are nearly insensitive to surface emissivity changes.

ACKNOWLEDGEMENTS

We thank Drs. Mircea Grecu and Robert Meneghini for their reviewing the paper and providing us with constructive comments. We thank Dr. Emmanuel Dinnat for his kind help with editing this paper. The author thanks Drs. Draine and Flatau for providing the author with the DDSCAT codes. Interest in our work by Dr. Ramesh Kakar of Code Y at NASA HQ and support from the Goddard Director's Discretionary Fund are also acknowledged. We thank NOAA-NESDIS for providing AMSU-B data. This work has been supported by NASA Grant NCC-5-584, S-69019-G, and NAG5-9668 and by the research project of the METRI/KMA, "A study on improving short-range precipitation forecast skill."

REFERENCES

Auer, A. H., and D. L. Veal, 1970: The dimension of ice crystals in natural clouds, *J. Amos. Sci.*, **27**, 919-926.

Bauer, P. and A. Mugnai, 2003: Precipitation profile retrievals using temperature-sounding microwave observations, *J. Geophy. Res.*, **108**, NO. D23, 4730, doi:10.1029/2003JD003572, 2003.

Bennartz, R. and G. W. Petty, 2001: The sensitivity of microwave remote sensing observations of precipitation to ice particle size distributions. *J. Appl. Meteor*., **40**, 345-364.

Bluestein, H. B. 1993: Synoptic-dynamic meteorology in midlatitudes. Oxford University press, 594.

Boucher, R. J. and J. G. Weiler, 1985: Radar determination of snowfall rate and accumulation. *J. Climate Appl. Meteorol.*, **24**, 68-73.

Calheiros, R. V. and I. Zawadski, 1987: Reflectivity-rain rate relationship for radar hydrology in Brazil. *J. Climate Appl. Meteorol*., **26**, 118-132.

Chen, F. W. and D. H. Staelin, 2003: AIRS/AMSU/HSP precipitation estimates. *IEEE Trans. Geosci. Remote Sensing*, **41**, 410-417.

Draine, B. T. (1988), The discrete dipole approximation and its application to interstellar graphite grains, *Astrophy. J.*, **333**, 848-872.

Draine, B. T. and P. J. Flatau, 2003: User Guide for the Discrete Dipole Approximation code DDSCAT 6.0.

Dudhia, J., 1993: A nonhydrostatic version of the Penn State/NCAR mesoscale model: Validation tests and simulation of an Atlantic cyclone and cold front. *Mon. Wea. Rev.*, **121**, 1493-1513.

Ferraro R. R., F. Weng, N. C. Grody, L. Zhao, H. Meng, C. Kongoli, P. Pellegrino, S. Qiu, and C. Dean, 2005: NOAA operational hydrological products derived from the advanced microwave sounding unit. **43**, 1036-1049.

Foster, J. L., C. Sun, J. P. Walker, R. Kelly, A. Chang, J. Dong, and H. Powell, 2005: Quantifying the uncertainty in passive microwave snow water equivalent observations. *Remote Sens. Env*., **94**,187-203.

Fujiyoshi, Y., T. Endoh, T. Yamada, K. Tsuboki, Y. Tachibana, and G. Wakahama, 1990: Determination of a Z-R relationship for snowfall using a radar and high sensitivity snow gauges. *J. Appl. Meteorol*., **29**, 147-152.

Foote, G. B., and P. S. DuToit, 1969: Terminal velocity of rain drops aloft. *J. Appl. Meteor*., **8**, 249-253.

Grell, G. A., J. Dudhia, and D. R. Stauffer, 1994: A description of the fifth generation Penn State/NCAR Mesoscale Model. NCAR Tech. Note NCAR/TN-3981STR, 138 pp.

Grenfell, T. C. and S. G. Warren, 1999: Representation of a nonspherical ice particle by a collection of independent spheres for scattering and absorption of radiation. *J. Geophy. Res*., **104**, 31697-31709.

Hewison, T. J. and S. J. English, 1999: Airborne retrievals of snow and ice surface emissivity at millimeter-wavelengths. *IEEE Trans. Geosci. Remote Sens*., **37**, 1871-1879.

Hewison, T. J., 2001: Airborne measurements of forest and agricultural and surface emissivity at millimeter-wavelengths. IEEE *Trans. Geosci. Remote Sens*., **39**, 393-400.

Heymsfield, A. J., 1972: Ice crystal terminal velocity, *J. Atmos. Sci.*, **29**, 1348-1357.

Heymsfield, A. J. and C. M. R. Platt, 1984: A parameterization of the particle size spectrum of ice clouds in terms of the ambient temperature and the ice water content, *J. Atmos. Sci*., **41**, 846-855.

Hogan, R. J., P. R. Field, A. J. Illingworth, R. J. Cotton, and T. W. Choularton, 2002: Properties of embedded convection in warm-frontal mixed-phase cloud from aircraft and polarimetric radar, *Q. J. R. Meteor. Soc*.,**128**, 451-476.

Houze, R. A., P. V. Hobbs, P. H. Herzegh, D. B. Parsons, 1979: Size distributions of precipitation particles in frontal clouds, *J. Atmos. Sci*., **36**, 156-162.

Kim, M. J., G. Skofronick-Jackson, and J.A.Weinman, 2004: Intercomparison of millimeter-wave radiative transfer models. *IEEE Trans. Geosci. Remote Sensing*, **42**, 1882-1890.

Kim, M.-J. 2004: A Physical Model to Estimate Snowfall over Land Using Microwave Measurements, Ph.D. Thesis, Atmospheric Sciences Department, University of Washington. Seattle, WA. pp 151

Kongoli, C., P. Pellegrino, R. Ferraro, N. Grody, and H. Meng, 2003: A new snowfall detection algorithm over land using measurements from the Advanced Microwave Sounding Unit (AMSU). *Geophys. Res. Lett*., **30**, 1756.

Liebe, H. J., P. Rosenkranz, and G. A. Hufford, 1992: Atmopsheric 60 GHz oxygen spectrum: New laboratory measurements and line parameters, *J. Quant. Spectrosc. Radiat. Transfer*, **48**, 629-643, 1992.

Liu, G. and J. A. Curry, 1996: Large-scale cloud features during January 1993 in the North Atlantic Ocean as determined from SSM/I and SSM/T2 observations. *J. Geoophys. Res*., **101**, 7019-7031.

Liu, G., and J. A. Curry, 2000: Determination of ice water path and mass median particle size using multichannel microwave measurements. J. Appl. Meteor. 38, 1182-1194.

Liu, G., 2004: Approximation of single scattering properties of ice and snow particles for high microwave frequencies. *J. Atmos. Sci*., **61**, 2441-2456.

Lo, K. K. and R. E. Passarelli, 1982: The growth of snow in winter storms: An airborne observational study, *J. Atmos. Sci*., **39**, 697-706.

Mätzler, C., U. Wegmüller, 1987: Dielectric properties of fresh-water ice at microwave frequencies, *J. of Physics D: Applied Physics*, **20**, 1623-1630.

Mishchenko, M. I., J. W. Hovenier, and L. D. Travis 2000: *Light scattering by nonspherical particles*, Academic press, 690 pp.

Moreau, E., P. Bauer, and F. Chevallier, 2003: Variational retrieval of rain profiles from spaceborne passive microwave radiance observations, *J. Geophy Res*., **108**, D16, 4521, doi:10.1029/2002JD003315

Noh, Y.-J., G. Liu, E.-K. Seo, and J. R. Wang 2006:Development of a snowfall retrieval algorithm at high microwave frequencies, *J. Geophy. Res*., **111**, D22216, doi:10.1029/2005JD006826.

Olson, W. S., C. D. Kummerow, G. M. Heymsfield, and L. Giglio, 1996: A method for combined passive-active microwave retrievals of cloud and precipitation profiles., *J. Appl. Meteor.*, **35**, 1763-1789.

Olson, W. S., C. D. Kummerow, S. Yang, G. W. Petty, W.-K. Tao, T. L. Bell, S. A. Braun, Y. Wang, S. E. Lang, D. E. Johnson and C. Chiu. 2006: Precipitation and latent heating distributions from satellite passive microwave radiometry. Part I: Improved method and uncertainties. *J. Appl. Meteor. and Climatol.*, **45**, 702-720.

Purcell, E. M. and C. R. Pennypacker, 1973: Scattering and absorption of light by nonspherical diectric grains. *Astrophy., J*. **186**, 705-714.

Rutledge, S. A. and P. V. Hobbs, 1983, The mesoscale and microscale structure and organization of clouds and precipitation in midlatitude cyclones. VIII: A model for the seeder-feeder process in in warm-frontal rainbands, *J. Atmos. Sci.*, **40**, 1185-1206.

Schols, J. L., J. A. Weinman, G. D. Alexander, R. E. Stewart, L. F. Angus, and A. C. Lee, 1999: Microwave properties of frozen precipitation around a North Atlantic cyclone. *J. Appl. Meteor*., **38**, 29-43.

Sekhon, R. S. and R. C. Srivastava, 1970: Snow size spectra and radar reflectivity. *J. Atmos. Sci.,* **28**, 944-983.

Skofronick-Jackson, G., M. -J. Kim, J. A. Weinman, and D. –E. Chang, 2004: A physical model to determine snowfall over land by microwave radiometry. *IEEE Trans. Geosci. Remote Sensing*, **42**, 1047-1058.

Smith, E. A., P. Bauer, F. S. Marzano, C. D. Kummerow, D. McKague, A. Mugnai, and G. Panegrossi, 2002: Intercomparison of microwave radiative transfer models for precipitating clouds. *IEEE Trans. Geosci. Remote Sensing*, **40**, 541-549.

Takano, Y. and K. N. Liou, 1988: Solar radiative transfer in cirrus clouds. Part I: Single scattering and optical properties of hexagonal ice crystals. *J. Atmos. Sci.,* **46,** 3-19.

Tao, W.- K. and J. Simpson, 1993: Goddard cumulus ensemble model. Part I: Model description, *Terres. Atmos. Ocean. Sci*., **4**, 35-72.

Tassa, A., S. Di Michele, A. Mugnai, F. S. Marzano, P. Bauer, J. P. V. P. Baptista , 2006 : Modeling uncertainties for passive microwave precipitation retrieval : evaluation of a case study. *IEEE Trans. Geosci. Remote Sensing*, **44**, 79-89.

Thomas, G. E. and K. Stamnes, 1999: Radiative transfer in the atmospheric and ocean, Cambridge Univ. Press, pp 517.

Vasiloff, S., R. M. Ramussen, M. Dixon, and F. Hage, 2000: Evaluation of snow forecasts provided by the Weather Support Deicing Decision Making (WSDDM) system. *Proc. 9th Conf. Aviation, Range Aerospace Meteorology,* Orlando, FL, 547-550.

Vivekanandan, J., V. N. Bringi, M. Hagen, and P. Meischner, (1994), Polarimetric radar studies of atmospheric ice particles. *IEEE Trans. Geosci. Remote Sens*., **32**, 1-10.

Vivekanandan, J., S. M. Ellis, R. Oye, D. S. Zrnic, A. V. Ryzhkov, and J. Straka, (1999), Cloud microphysics retrieval using S-band dual-polarization radar measurements. *Bull. Amer. Meteor. Soc*., **80**, 381-388.

Weinman, J. A. and R. Davis, 1978: Thermal microwave radiances from horizontally finite clouds of hydrometeors, *J. Geophy. Res*., **83**, 3099-3107.

Weinman, J. A. and I. M. Hakkarinen, 1990: Determination of maritime snowfall from radar and microwave radiometer measurements. *Proc. AMS. Conf. Cloud Physics*, San Francisco, CA, 1990.

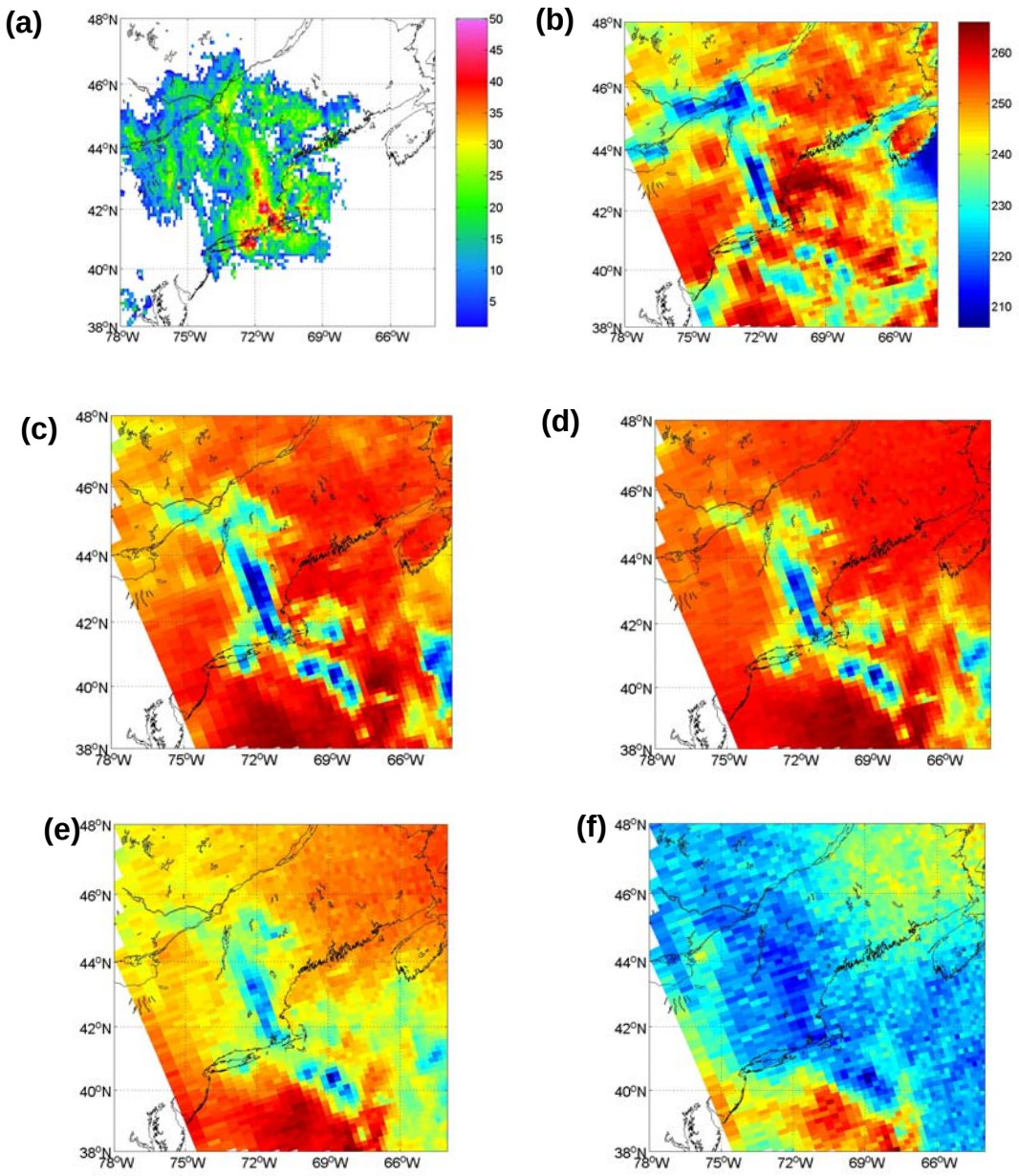

Figure 1. (a) Radar reflectivity (dBZ) obtained from the NWS operational radar composite at variable heights between 0.5 and 2.5 km measured at 2300 UTC on March 5, 2001. Note that heavy snowfall over CT, MA, NH, and VT. Tbs (K) observed from (b) 89 GHz, (c) 150 GHz, (d) 183.3 ± 7 GHz, (e) 183.3 ± 3 GHz, and (f) 183.3 ± 1 GHz of AMSU-B at 23:02 UTC on March 2001. The color scale shown in (b) applies to the subsequent figures.

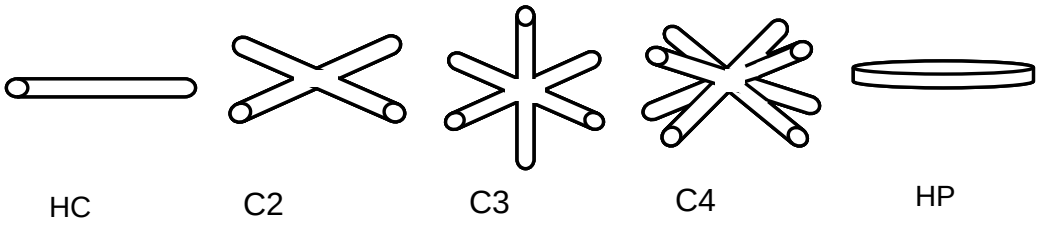

Figure 2. Model crystal habits considered in this study.

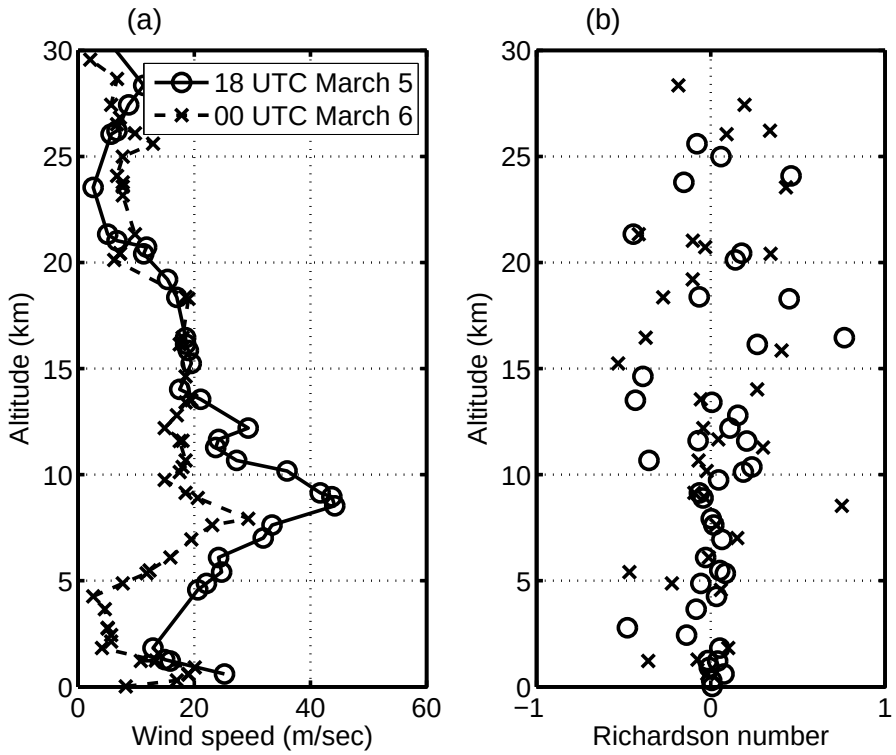

Figure 3. Profiles of (a) wind speed and (b) Richardson number measured in Brookhaven, NY at 18 UTC on March 5 and 00 UTC on March 6, 2001 during the New England blizzard.

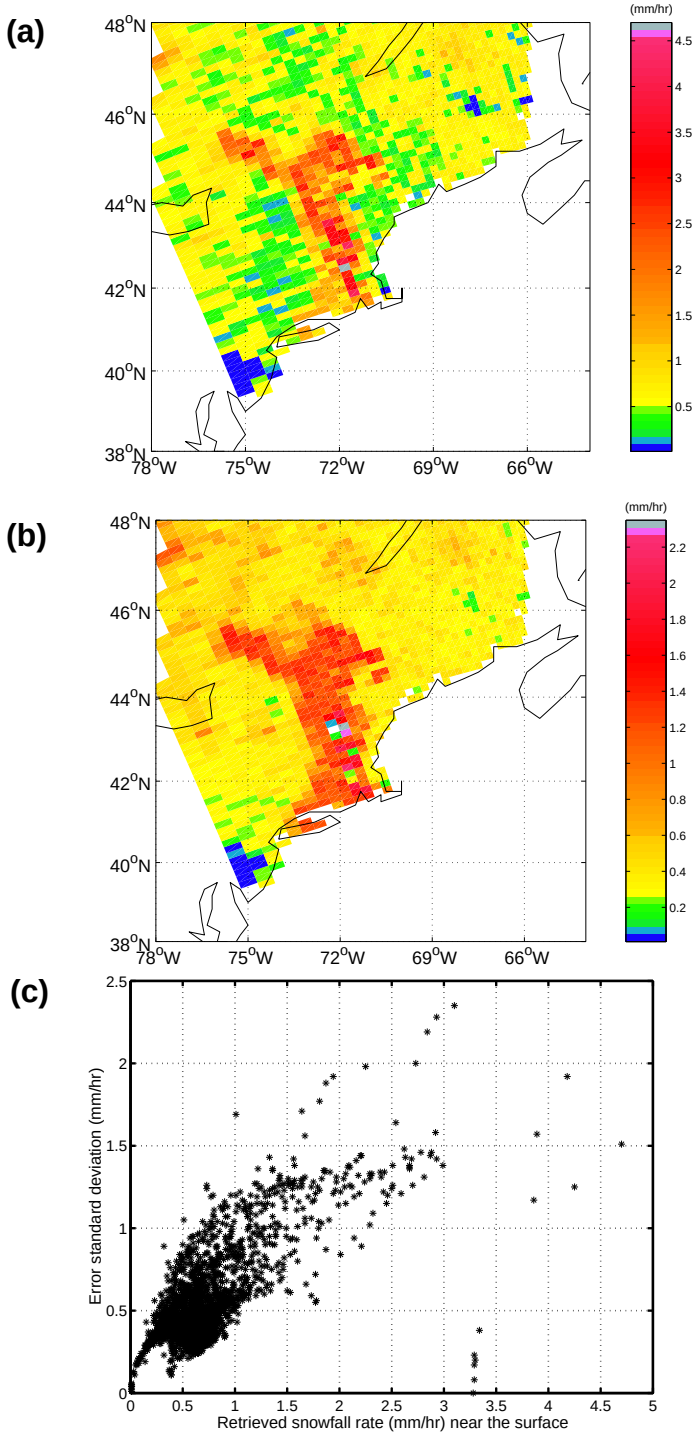

Figure 4. Retrieved (a) water equivalent snowfall rate (mm/hr) and (b) uncertainty estimate (mm/hr) at 0.02 km altitude. Since the retrievals are applied to precipitation over land, the oceanic 1regions are masked.

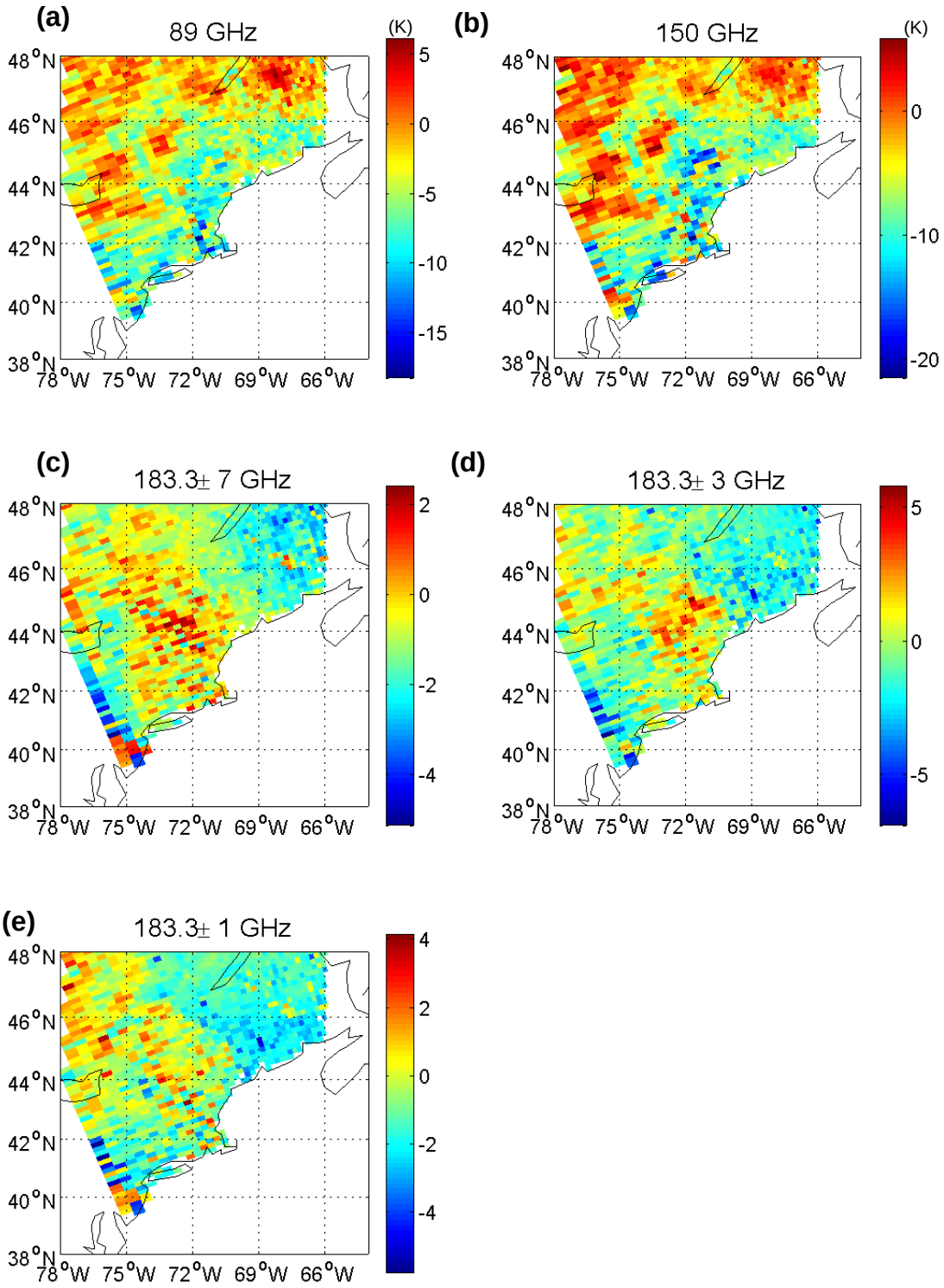

Figure 5. Departures of estimated brightness temperatures from measured brightness temperatures: Tb(estimated) – Tb(measured) (K) at (a) 89 GH,z (b) 150 GHz, (c) 183.3 ± 7 GHz, (d) 183.3 ± 3 GHz, and (e) 183.3 ± 1 GHz.

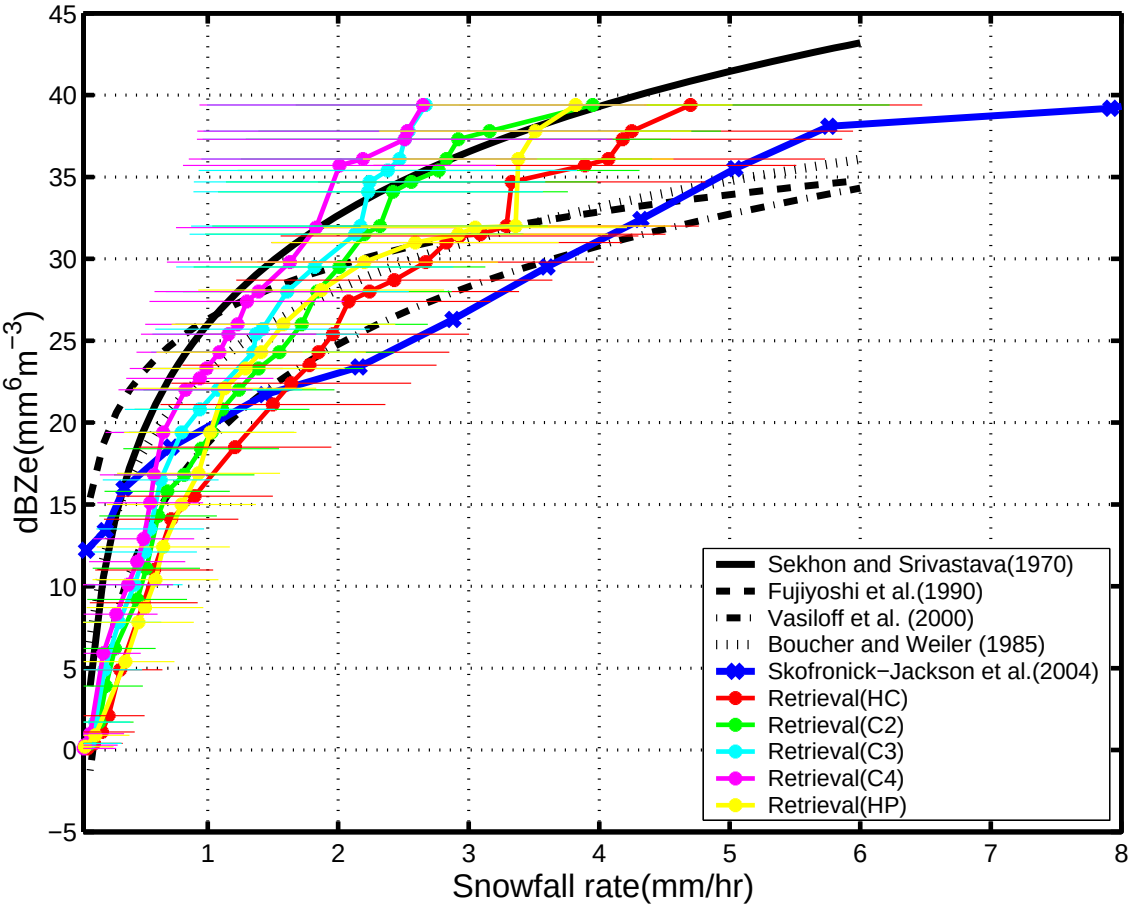

Figure 6. Measured NWS radar reflectivity Z_e versus retrieved snowfall rate (mm/hr) using different snow particle models. Results are compared with previously published Z_e-R relationships for falling snow. The uncertainty values of snowfall rates retrieved different snow particle models are shown as error bars.

(a)

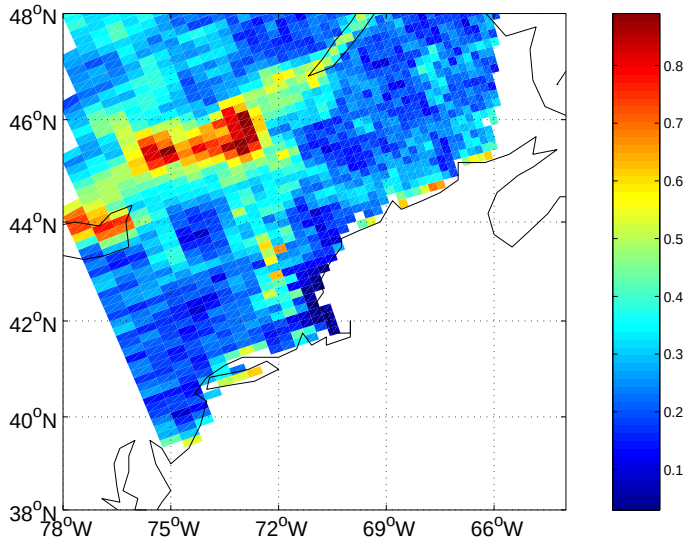

(b)

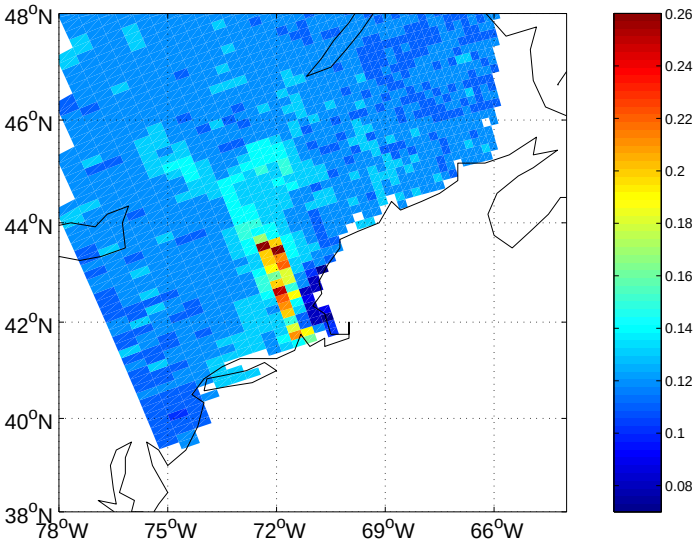

Figure 7. Retrieved (a) fraction of snow cover on the ground and (b) its uncertainty estimate.

1

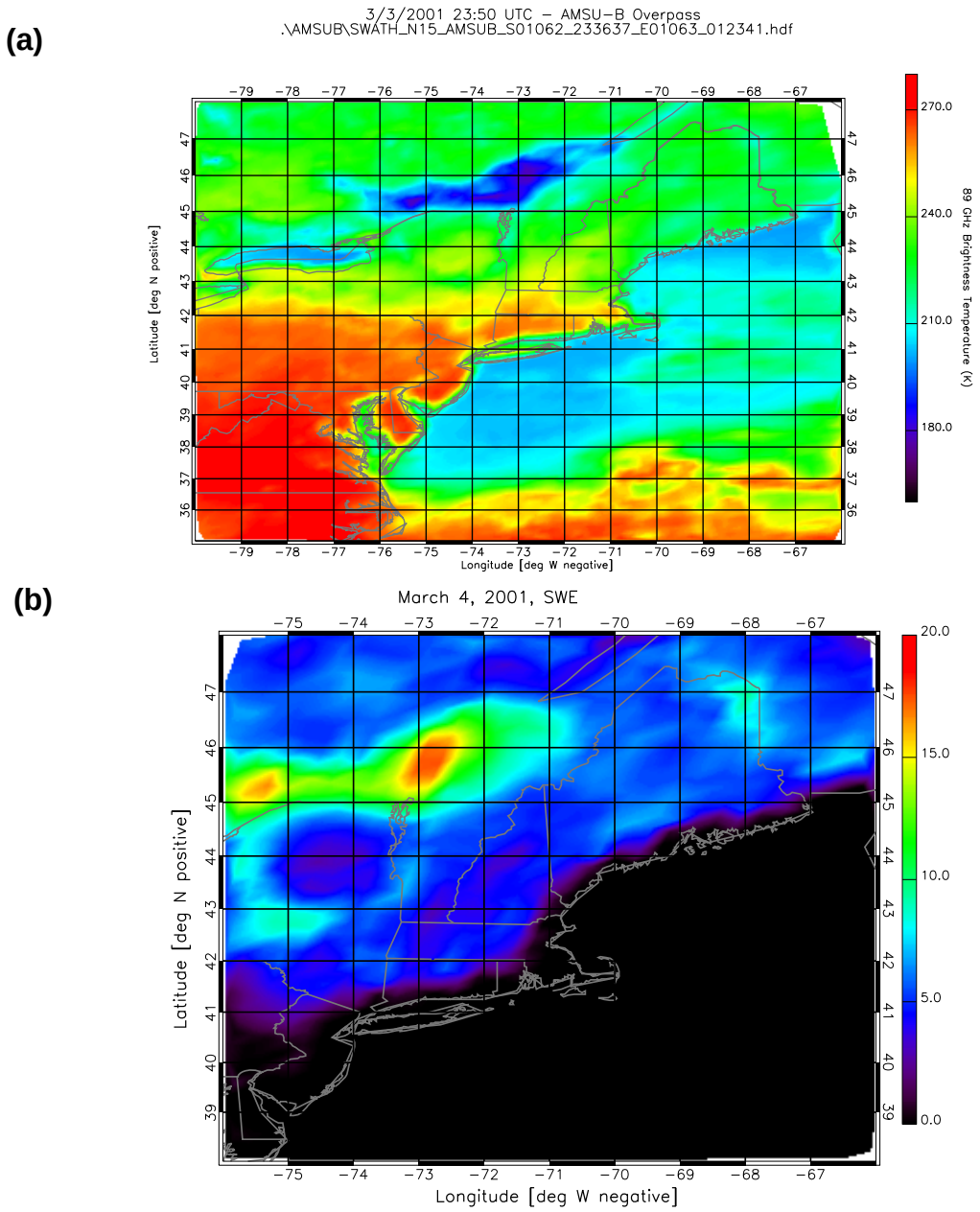

Figure 8. (a) The 89 GHz AMSU-B channel image on March 3, 2001. (b) Distribution of snow water equivalent (SWE) derived with the algorithm in Foster et al. (2005) using the SSM/I 19 GHz and 37 GHz vertically polarized channels, over the area of interest on March 4, 2001.

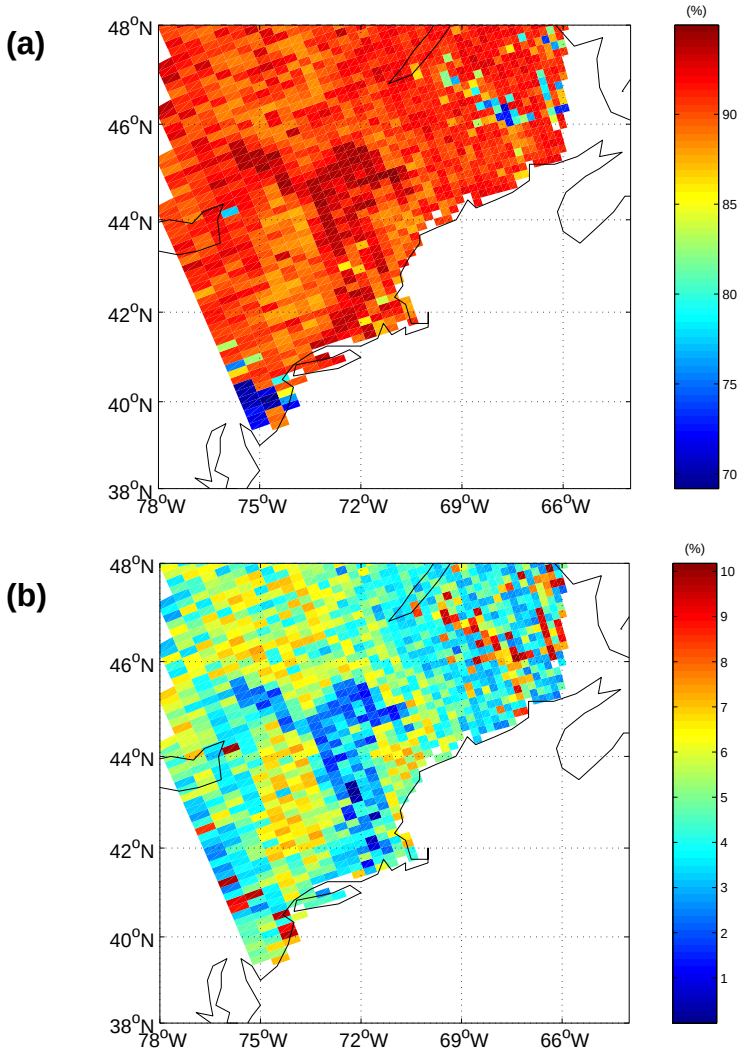

Figure 9. Retrieved (a) relative humidity (%) and (b) uncertainty estimate at 0.02 km altitude. Since the retrievals are applied to precipitation over land, the oceanic regions are masked.

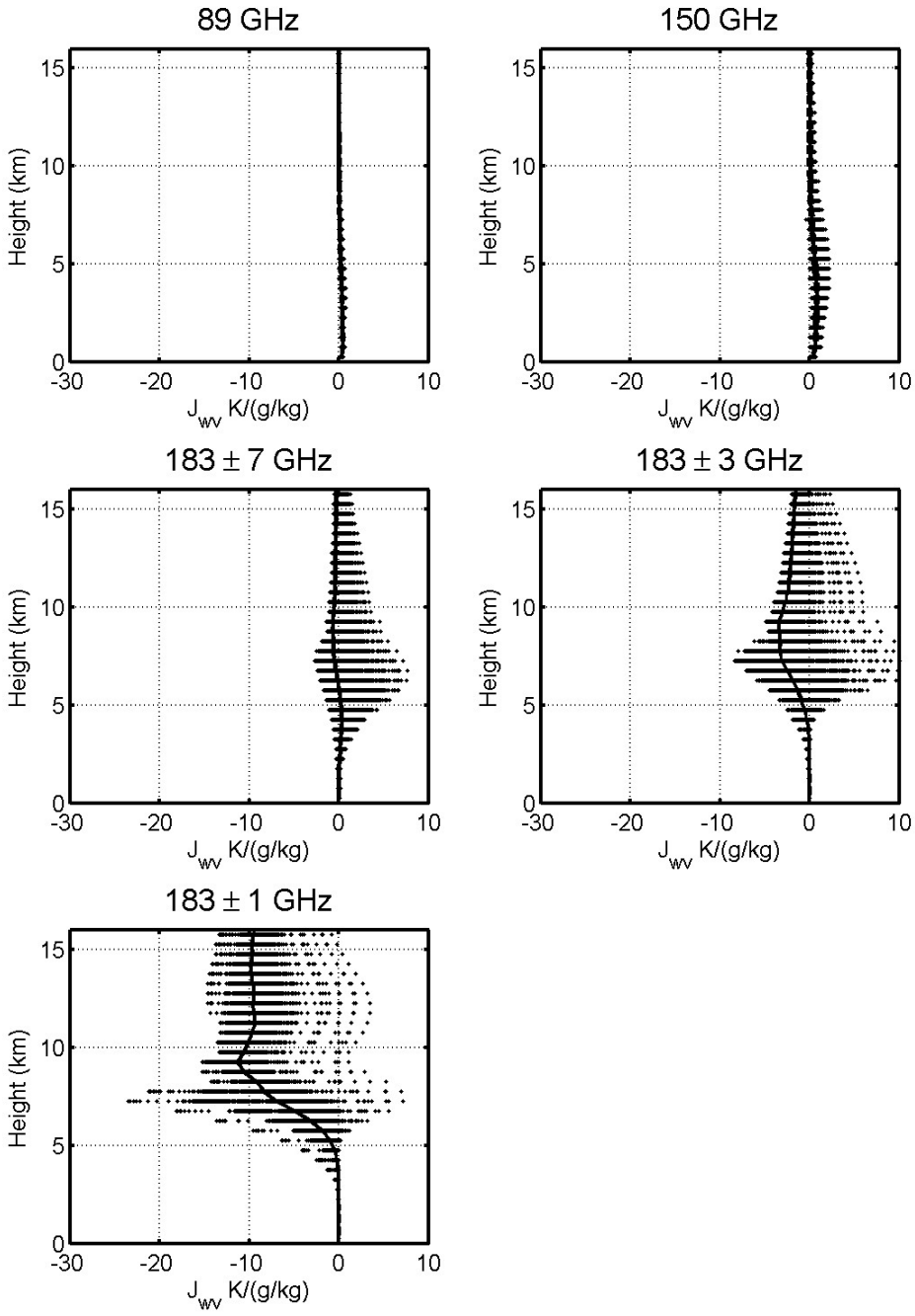

Figure A1. Jacobians for AMSU-B channels with respect to water vapor mixing ratio.

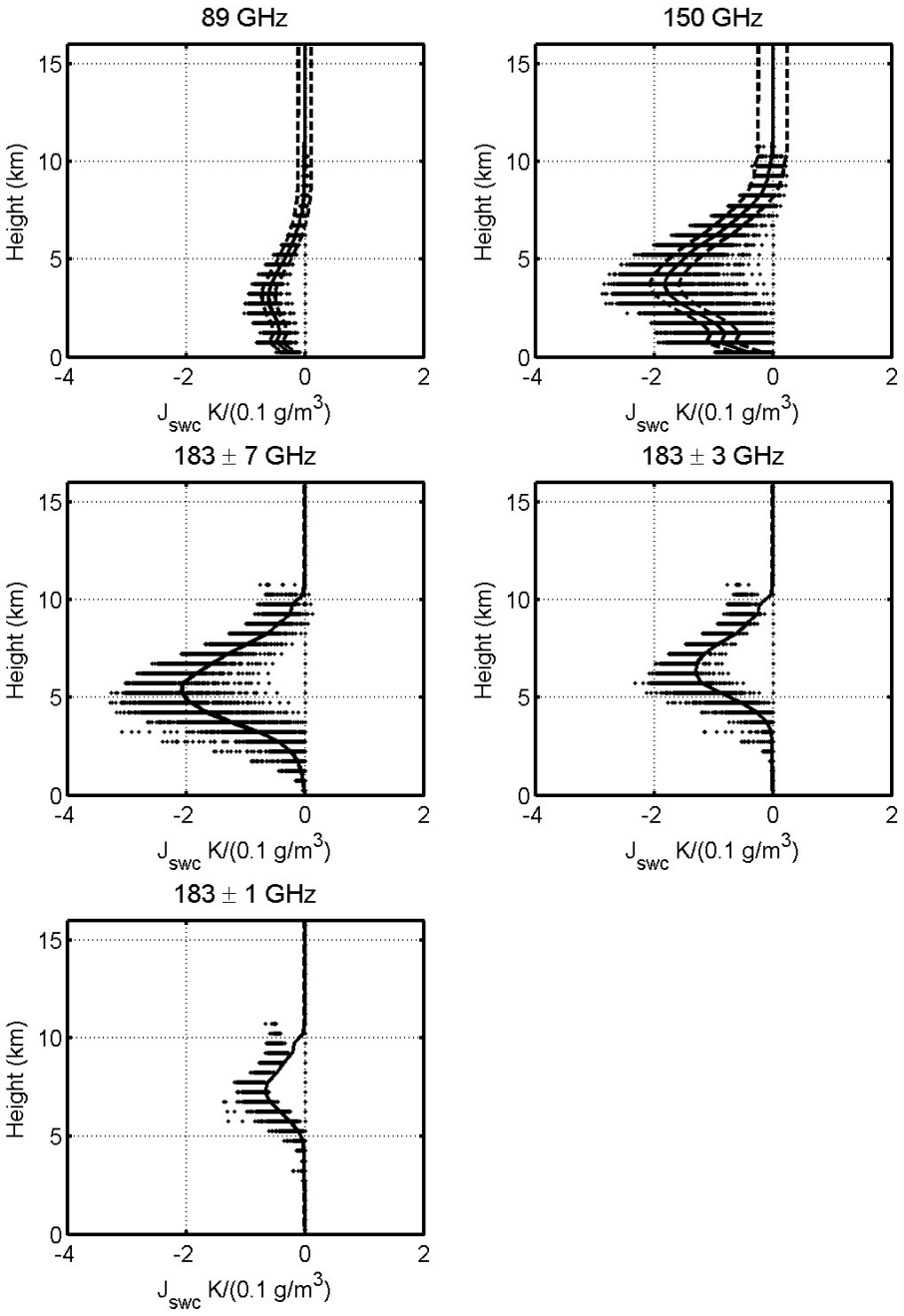

Figure A2. Jacobians for AMSU-B channels with respect to snow water content (swc).

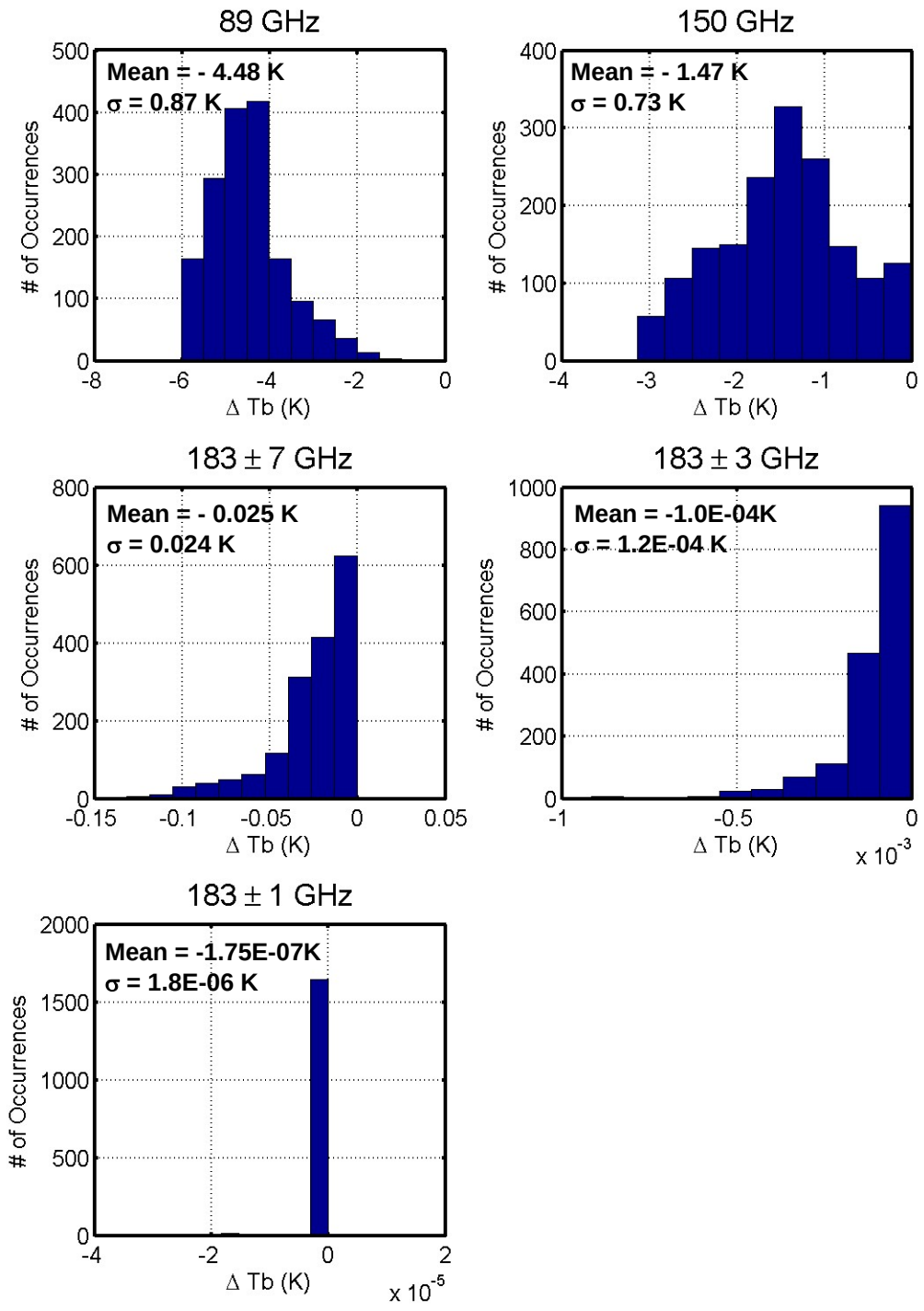

Figure A3. Histograms of calculated Tb differences when the fraction of surface snow coverage increases from **f** = 0.5 to **f** = 0.6.